Electron Paramagnetic Resonance Investigations of Lanthanide-Doped Barium Titanate: Dopant Site Occupancy

Timothy D. Dunbar,*,†,‡ William L. Warren,†,§ Bruce A. Tuttle,† Clive A. Randall,|| and Yoed Tsur||,⊥

Materials and Process Sciences, Sandia National Laboratories, Albuquerque, New Mexico 87185, and Materials Research Institute, The Pennsylvania State University, University Park, Pennsylvania 16802

Received: August 26, 2003; In Final Form: October 21, 2003

Air-fired barium titanate samples doped with cerium, neodymium, samarium, gadolinium, dysprosium, erbium, or ytterbium were examined by electron paramagnetic resonance (EPR). Reducing atmosphere-fired europium-doped barium titanate was also investigated with EPR. Each dopant was studied in both Ba- and Ti-rich (Ba/Ti = 1.01, 0.99) samples. Point charge calculations were used to predict the EPR spectrum of each lanthanide in A- and B-sites. Different EPR spectra are expected for A- versus B-site substitution when Ce^{3+}, Sm^{3+}, Dy^{3+}, and Yb^{3+} are the dopants. The experimentally observed Ba/Ti doping behavior of Ce^{3+} in $BaTiO_3$ suggests that as a 3+ cation it is on the A-site. No EPR active signal was observed for Sm^{3+} in $BaTiO_3$. Eu^{2+} and Gd^{3+}, as previously discussed in the literature, were found to be an A-site dopant and amphoteric, respectively. Dy^{3+} was found to be a B-site dopant with an EPR signal intensity suggesting amphoteric behavior, whereas Yb^{3+} showed only B-site occupancy. Nd^{3+} and Er^{3+} could not easily be assigned to a particular site by EPR methods alone. We also discuss the lanthanide dopant's effect on the observed levels of titanium vacancies, barium vacancies, and Mn^{2+} impurities.

Introduction

Barium titanate, doped with lanthanide ions, has found use as the dielectric of multilayer ceramic capacitors. When the capacitors are fired in low oxygen partial pressures, certain lanthanides, such as Ho, Dy, and sometimes Er, can improve the resistance of the barium titanate to electrochemical or time dependent failure.[1] It is thought that these "magic" dopants can choose their site occupancy as a result of the local Ba/Ti ratio and oxygen partial pressure during firing.[2,3] Such dopants are also termed "amphoteric" because the site change of a well-defined valence dopant causes a change of the relative charge.[4]

Dopant site location has been determined previously in $BaTiO_3$ by a variety of techniques, including X-ray diffraction (XRD),[5−8] atomistic simulations,[9,10] conductivity measurements,[4] luminescence,[11] and electron paramagnetic resonance (EPR).[12−14] We have used EPR to investigate a series of lanthanide-doped barium titanates, with the chief aim of determining the site occupancy of the lanthanide. To facilitate the detection of amphotericity, we have studied samples that are either barium-rich or titanium-rich (Ba/Ti = 1.01 or 0.99, respectively). Ba-rich samples will drive amphoteric dopants to more frequently occupy B-sites, and Ti-rich samples will drive such dopants more frequently into the A-sites. We have chosen ions with an odd number of electrons (Kramers ions) on the basis of the fact that non-Kramers ions generally have such short relaxation times as to make their EPR signals too broad to detect. Our goal with these EPR studies is to complement recent X-ray diffraction investigations to access details of site occupancy and also establish further details in associated cationic vacancies.[6,7] Though one can use ionic radii to predict ion substitution behavior in a crystalline structure, one cannot rely on it alone, as several examples exist in which such arguments predict the wrong site occupancy.[15−17]

We address the question of lanthanide dopant location through a combination of simple calculations and EPR experiments on $BaTiO_3$ powders. Our analytical calculations use a point charge model to determine the cubic crystalline electric field parameters for both A- and B-site locations for each particular lanthanide dopant. We then can predict the fundamental lowest energy level of the 3+ lanthanide in both types of site. This then allows us to assess whether A- or B-site dopant locations will have different EPR spectra. We then compare our predicted results with the actual EPR spectra collected from Ba- or Ti-rich $BaTiO_3$ powders. Dopant locations from the EPR results are then compared to those determined via room-temperature X-ray diffraction. Finally, we also interpret these results and the observed levels of common defects (titanium and barium vacancies) and impurity ions (Mn^{2+}) in the context of the known defect chemistry of barium titanate.[18,19]

Theory, Theoretical Results, and Discussion

For lanthanide ions, interaction with the crystalline electric field is much weaker than the spin−orbit coupling.[20] This is expressed as a Hamiltonian with a sum of all interactions such that

$$H = H_{fi} + H_{so} + H_{cf} + H_z + H_{hf} \quad (1)$$

* Corresponding author. E-mail: tddunbar@mmm.com.
† Sandia National Laboratories.
‡ Current address: Corporate Materials Laboratory, 3M Co., 3M Center 201-1W-28, St. Paul, Minnesota, 55144, Phone: (651) 737-2856. Fax: (651) 736-5381.
§ Current address: Sciperio, Inc., 5202-2 N. Richmond Hill Road, Stillwater, OK 74075.
|| The Pennsylvania State University.
⊥ Current address: Chemical Engineering department, Technion, Israel Institute of Technology, Haifa, Israel.

10.1021/jp036542v CCC: $27.50
Published on Web 12/24/2003

where $H_{fi} + H_{so} >> H_{cf} >> H_z + H_{hf}$, H_{fi} is the Hamiltonian of the free ion, H_{so} is the spin−orbit Hamiltonian, H_{cf} is the crystal field Hamiltonian, H_z is the Zeeman Hamiltonian, and H_{hf} is the hyperfine Hamiltonian. The crystalline electric field is thus a perturbation on the $2J + 1$ degeneracy of the free-ion ground state. The action of the crystal field upon the free ion can partially remove the degeneracy from among the various Γ_i states. The crystal field Hamiltonian in cubic symmetry can be written as

$$H_{cf} = B_4(O_4^0 + 5O_4^4) + B_6(O_6^0 - 21O_6^4) \quad (2)$$

where O_l^m are the equivalent operators and B_4 and B_6 are coefficients that determine the strength of the electric field.[20] In general, B_4 and B_6 depend on the type of coordination (12-fold or 6-fold in the case A- or B-sites in $BaTiO_3$) and the particular J manifold involved. Because of their J dependence, these coefficients are often different for the various 3+ rare earth ions.

Lea, Leask, and Wolf (LLW) performed calculations that detail the Γ_i energy levels for possible ratios of the fourth- and sixth-order coefficients.[21] To bring the coefficients into the same numerical range, the LLW method separates out factors common to all matrix elements. Following convention, we define

$$b_4 = B_4F_4 = Wx \quad (3)$$

$$b_6 = B_6F_6 = W(1 - |x|) \quad (4)$$

where F_4 and F_6 are constants and $-1 < x < +1$. The cubic crystal field Hamiltonian then becomes

$$H_{cf} = W\left[x\frac{(O_4^0 + 5O_4^4)}{F_4} + (1 - |x|)\frac{(O_6^0 - 21O_6^4)}{F_6}\right] \quad (5)$$

Consequently, if one can determine the ratio b_4/b_6, one can then find x and the sign of W, and can then predict the fundamental level, Γ_i.

For our simple point charge model, we follow the calculation methodology of Bureau et al.[22] The contribution to the fourth- and sixth-order coefficients resulting from a single coordination sphere, k, were expressed as

$$b_{4,k} = -F_4C_{4,k}\frac{e^2}{4\pi\epsilon_0}\frac{\langle r^4\rangle a_4}{r_k^5}Z^k \quad (6)$$

and

$$b_{6,k} = -F_6C_{6,k}\frac{e^2}{4\pi\epsilon_0}\frac{\langle r^6\rangle a_6}{r_k^7}Z^k \quad (7)$$

$C_{4,k}$ and $C_{6,k}$ are constants, unique to each type of coordination sphere; $\langle r^4\rangle$ and $\langle r^6\rangle$ are the fourth- and sixth-order ionic radii;[20] r_k is the radius of the coordination sphere (distance from the dopant to an ion in the sphere); a_4 and a_6 are the multiplicative factors for 4f ions;[20] and Z^k is the charge of an ion in the coordination sphere. The terms b_4 and b_6 can then be found by summing $b_{4,k}$ and $b_{6,k}$ over all possible shells. Because we are performing these calculations for six different lanthanides, it is useful to factor out all the lanthanide-specific parameters that do not change as a function of k. This yields

$$b_4 = \sum^k b_{4,k} = \kappa_4\sum^k C_{4,k}\frac{1}{r_k^5}Z^k \quad (8)$$

where

$$\kappa_4 = -F_4\langle r^4\rangle a_4\frac{e^2}{4\pi\epsilon_0}$$

and

$$b_6 = \sum^k b_{6,k} = \kappa_6\sum^k C_{6,k}\frac{1}{r_k^7}Z^k \quad (9)$$

where

$$\kappa_6 = -F_6\langle r^6\rangle a_6\frac{e^2}{4\pi\epsilon_0}$$

From the equations set forth by Bureau et al.,[22] it can be shown that the constants $C_{4,k}$ and $C_{6,k}$ can be evaluated according to the following expressions

$$C_{4,k} = \frac{\sqrt{\pi}}{12}\sum_{i=1}^N Y_4^0(\theta_i,\phi_i) \quad (10)$$

and

$$C_{6,k} = \frac{1}{8}\sqrt{\frac{\pi}{13}}\sum_{i=1}^N Y_6^0(\theta_i,\phi_i) \quad (11)$$

where N is the total number of ions, i, in each shell, k, and $Y_l^m(\theta_i,\phi_i)$ is a spherical harmonic.

For our $BaTiO_3$ calculations, we set the lattice constant, a_0, equal to 4.004 Å.[23] Although $BaTiO_3$ is rhombohedral at 10 K (the EPR measurement temperature), the ion displacement relative to the cubic prototype is quite small.[24] Consequently, the use of cubic symmetry is an appropriate approximation.

A computer program was written to calculate

$$\sum^k C_{4,k}\frac{1}{r_k^5}Z^k$$

and

$$\sum^k C_{6,k}\frac{1}{r_k^7}Z^k$$

for either A- or B-site substitution in $BaTiO_3$. The program evaluates the spherical harmonics for each particular shell around either type of site. Figure 1 shows the first three coordination spheres around a lanthanide in A- and B-sites, respectively. Table 1 shows the shell data for the first three fourth- and sixth-order terms for A-site substitution, and Table 2 shows the same for B-site substitution. It is clear from Figure 2 that the fourth-order B-site and both sixth-order sums converge more quickly than does the fourth-order A-site sum. The fourth-order A-site sum as a function of shell number is, relative to its initial value, closer to zero than for any of the other three sums. This "quasi

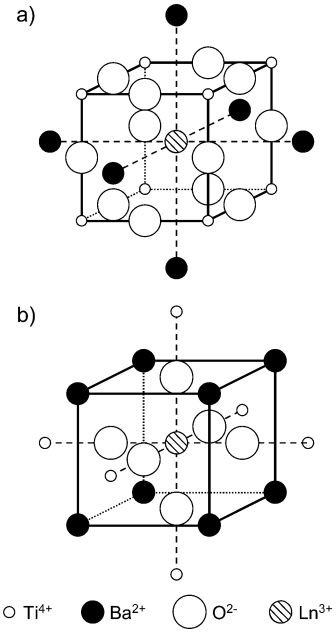

Figure 1. Nearest neighbors of a lanthanide dopant when it is an A-site, substituting for Ba^{2+} (a) or a B-site, substituting for Ti^{4+} (b).

TABLE 1: A-Site Calculation Data, for $a_0 = 4.004$ Å

k	atom	r_k	Z^k	$C_{4,k}(1/r_k^5)Z^k$ (Å^{-5})	$C_{6,k}(1/r_k^7)Z^k$ (Å^{-7})
1	O^{2-}	$\sqrt{2}/(2)a_0$	−2	2.41×10^{-3}	2.09×10^{-4}
2	Ti^{4+}	$(\sqrt{3}/2)a_0$	+4	-3.10×10^{-3}	7.37×10^{-5}
3	Ba^{2+}	a_0	+2	8.50×10^{-4}	5.68×10^{-6}

TABLE 2: B-Site Calculation Data, for $a_0 = 4.004$ Å

k	atom	r_k	Z^k	$C_{4,k}(1/r_k^5)Z^k$ (Å^{-5})	$C_{6,k}(1/r_k^7)Z^k$ (Å^{-7})
1	O^{2-}	$(1/2)a_0$	−2	-2.72×10^{-2}	-7.27×10^{-4}
2	Ba^{2+}	$(\sqrt{3}/2)a_0$	+2	-1.55×10^{-3}	3.69×10^{-5}
3	Ti^{4+}	a_0	+4	1.70×10^{-3}	1.14×10^{-5}

cancellation" has been noted before in calculations on $SrTiO_3$.[25] For A-site substitution,

$$\sum^{k} C_{4,k} \frac{1}{r_k^5} Z^k$$

converges to 3.19×10^{-4} Å^{-5} and

$$\sum^{k} C_{6,k} \frac{1}{r_k^7} Z^k$$

converges to 2.84×10^{-4} Å^{-7}, whereas for B-site substitution, the sums converge to -2.75×10^{-2} Å^{-5} and -6.75×10^{-4} Å^{-7}, respectively.

For the calculation of the κ_4 and κ_6, LLW have determined F_4, F_6, a_4, and a_6,[21] whereas Abragam and Bleaney have compiled $\langle r^4 \rangle$ and $\langle r^6 \rangle$.[20] To calculate b_4 or b_6 for a particular lanthanide in a particular site, one multiplies the proper order constant (κ_4 or κ_6) by the series sum for that site location. For example, to find b_4 for Nd^{3+} in an A-site, we take 381.9 cm^{-1} Å^5 × 3.19×10^{-4} Å^{-5} = 0.122 cm^{-1}. Table 3 details the results of the calculations and shows the predicted lowest energy state and g value (if relevant). Once b_4 and b_6 are calculated, it is straightforward to find x and W. Upon solving for these values, the tables of LLW[21] can be consulted for each particular J manifold to find the ground state. It is then possible to determine the appropriate g value.[20]

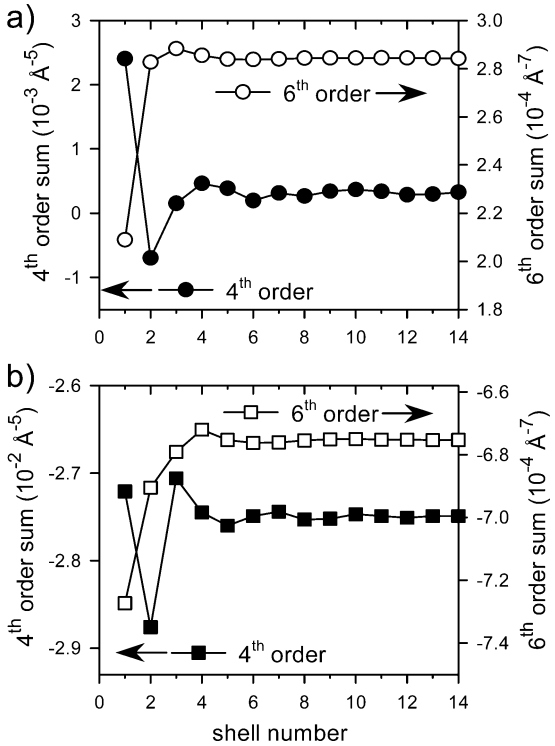

Figure 2. Plot of the fourth-order sum, $\Sigma^k C_{4,k}(1/r_k^5)Z^k$, and the sixth-order sum, $\Sigma^k C_{6,k}(1/r_k^7)Z^k$, as a function of shell number for A-site (a) or B-site (b) substitution.

In general, the predicted ground state is rather insensitive to the input parameters. Only in the case of Nd substituted into the B-site of $BaTiO_3$ does the calculated x value fall close to where two states (Γ_6 and Γ_8) cross. Thus, in the majority of cases, our calculation of the appropriate ground state should not be overly affected by errors typical to point charge calculations such as lattice relaxations[20] and expansion of the lanthanide 4f radial wave function,[26] among others.[27] Given that the above calculated ground states are correct, it is important to note additional factors that can change the EPR spectrum from what one would predict. When levels are spaced closely, such as for Ce^{3+}, admixing of the ground state with higher states can shift the predicted g value.[12] Also, local charge compensation can lower the symmetry of a particular site. It is possible that an ion in a cubic site with a Γ_8 ground state could have its symmetry lowered by local charge compensation such that the Γ_8 quartet splits into several states, one of which would then be the ground state.

We note here that the two S-state ions in this study, Eu^{2+} and Gd^{3+} are minimally affected by the crystal field.[20] As a consequence, it is not possible to predict the effect of the crystal field upon the EPR spectra for either A- or B-site substitution.

Experimental Section

Preparation details of the 1% lanthanide-doped barium titanate ceramics are given elsewhere.[6] Barium carbonate (99.98%), titanium dioxide (99.99%), and the appropriate rare earth oxide (>99.9%) were mixed in a ball mill with 500 weight ppm silica, then dried, compacted, and calcined at 1200 °C in air for 2 h. This material was ground, binder was added, and the mixture compacted. The binder was burned out at 800 °C. Sintering was done at 1400 °C for 2 h either in air (Ce, Nd, Sm, Gd, Dy, Er, and Yb samples) or a reducing atmosphere, established by an $N_2/H_2/H_2O$ mixture, $P(O_2) \sim 10^{-10}$ atm, as monitored by zirconia probe (Eu sample). These ceramic pellets were then

TABLE 3: Calculation Results for Non-*S*-State Lanthanides: κ_4, κ_6, b_4, b_6, *x*, and *W* Values, Predicted Ground States, and *g* Values

ion	κ_4 (cm^{-1} Å^5)	κ_6 (cm^{-1} Å^7)	site	b_4 (cm^{-1})	b_6 (cm^{-1})	x	W	ground state	g value
Ce^{3+}	−11990	0	A	−3.82	0	−1	+	Γ_8	
			B	330	0	1	+	Γ_7	1.429
Nd^{3+}	381.9	3026	A	0.122	0.861	0.12	+	Γ_6	2.667
			B	−10.5	−2.04	0.84	−	Γ_6	2.667
Sm^{3+}	−2593	0	A	−0.827	0	−1	+	Γ_8	
			B	71.3	0	1	+	Γ_7	1.429
Dy^{3+}	42.77	−186.7	A	0.0136	−0.0531	−0.20	−	$\Gamma_8^{(3)}$	
			B	−1.176	0.126	−0.90	+	Γ_6	6.667
Er^{3+}	−27.32	−291.1	A	−0.00871	−0.0828	0.10	−	$\Gamma_8^{(3)}$	
			B	0.751	0.197	0.79	+	$\Gamma_8^{(1)}$	
Yb^{3+}	908.4	−1476	A	0.290	−0.420	−0.41	−	Γ_8	
			B	−25.0	0.997	−0.96	+	Γ_6	2.667

crushed into powders. Equal weights of each powder were weighed into individual quartz tubes.

EPR spectra at room temperature and temperatures as low as 10 K were taken on Bruker ESP300e and Bruker EMX X-band spectrometers, each equipped with flow-through liquid He cryostats (Oxford). Microwave frequencies were measured using a Hewlett-Packard 5342A automatic frequency counter. All samples were carefully checked for power saturation effects, and at a microwave power of 0.6 mW, none was observed.

Powder pattern simulations and other modeling of the experimental spectra were performed using a combination of WinEPR (Bruker), Simfonia (Bruker), and home-written software.

Results

Experimental observations regarding each lanthanide in barium titanate are listed below and discussed in context of the theoretical prediction of lowest energy state for A- or B-site occupancy.

Ce^{3+}-Doping. The theory discussed above predicts that there should be different spectra for Ce^{3+} ($4f^1$ with $^2F_{5/2}$) in the A-site (Γ_8 state) versus the B-site (Γ_7 state, $g = 1.429$) of barium titanate. Previous EPR observations of Ce^{3+} codoped with Rh^{4+} in $BaTiO_3$ revealed the symmetry of the Ce^{3+} ion to be trigonal, rather than cubic.[12] Furthermore, admixing of higher states has been implicated in the large differences between calculated and experimental *g* values.[28] Our calculations, then, are valid only in a general way to Ce^{3+}.

Experimentally, we observed broad signals (see Figure 3) that powder pattern simulations indicate are in close agreement with the previously reported results for Ce^{3+} in $BaTiO_3$, namely, $g_\perp = 1.36$ and a $g_\parallel = 0.88$.[12] Cerium has been reported to be a multivalent cation, and will likely be incorporated as 3+ on the A-site and 4+ on the B-site.[29] On the basis of the low intensity of the signals observed, one may be tempted to specify that most of the Ce in these samples is Ce^{4+}, but it should be noted that the integrated intensity of powder pattern spectra with widely separated $g_\perp$ and $g_\parallel$ (such as these) can be quite high because of the breadth of magnetic field over which one integrates.

Figure 3 shows that the Ba-rich sample has about 60% of the Ce^{3+} signal as does the Ti-rich one. This difference follows the simple rationale that having more Ba present prevents Ce from occupying the A-site as a 3+ ion and forces it to the B-site where, in an oxidative environment, it will be a 4+ ion. This observation supports assigning the observed Ce^{3+} to the A-site location.

In Figure 4 we show a spectrum that focuses upon the signals near $g = 2$. We see three main types of signal. Foremost is the large, slightly anisotropic signal at $g = 2.004$. Though features

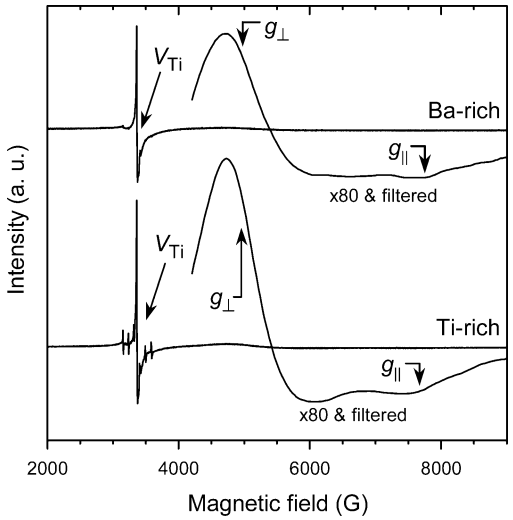

Figure 3. EPR spectra of Ce-doped $BaTiO_3$ at 10 K, where either Ba/Ti = 1.01 or 0.99. The features at $g_\perp = 1.36$ and $g_\parallel = 0.88$ result from Ce^{3+}. The filtered spectra are obtained by performing a Fourier transform, scaling the transformed spectrum by an exponential function to remove high-frequency noise, then performing the inverse Fourier transform.

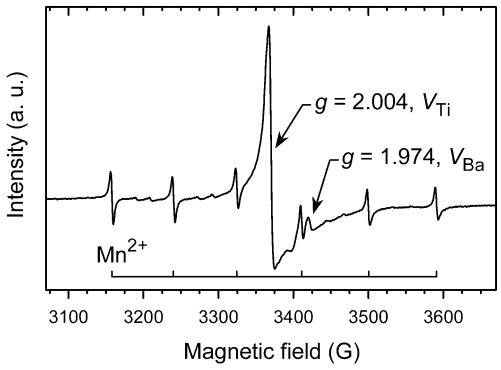

Figure 4. EPR spectra of Ce-doped Ti-rich $BaTiO_3$ at 10 K, showing signals from V_{Ti}, V_{Ba}, and Mn^{2+}.

near $g = 2$ have often been assigned to Fe^{3+},[30] we did not see any of the other resonances ($g = 6.26$, 5.54, 2.47, and 1.62) also observed when Fe^{3+} is responsible for the $g = 2$ signal.[31] Consequently, in accord with Kolodiazhnyi and Petric, we assigned this feature to titanium vacancies (V_{Ti}) with unpaired electron spin (e.g., V'_{Ti} and V'''_{Ti}).[32] The second feature of importance is the small signal at $g = 1.974$. Although some authors have assigned signals with *g* values close to this ($g = 1.963-1.975$) to $Ti^{3+}-Ln^{3+}$ complexes,[33] we assigned it to an ionized barium vacancy (V_{Ba})[32] for two reasons. First, unlike $Ti^{3+}-Ln^{3+}$ complexes its *g* value remained constant at 1.974

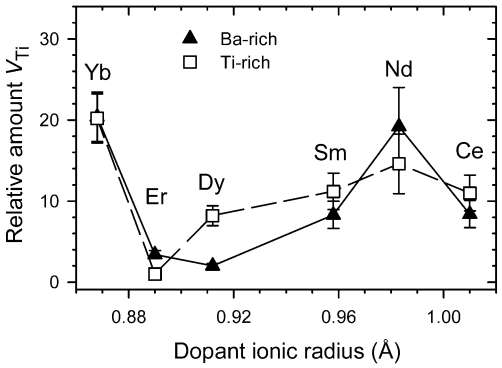

Figure 5. Relative amounts of V_{Ti} in Ba- or Ti-rich lanthanide-doped $BaTiO_3$ samples, scaled so that the amount of V_{Ti} in Er-doped Ti-rich $BaTiO_3$ is equal to 1.

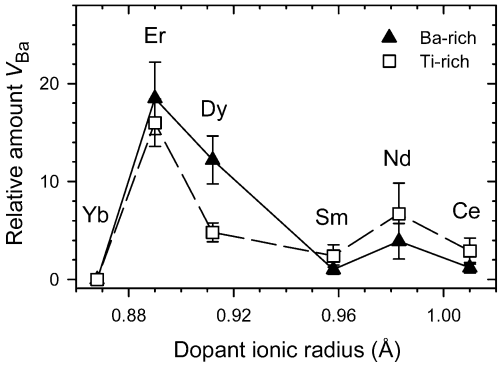

Figure 6. Relative amounts of V_{Ba} in Ba- or Ti-rich lanthanide-doped $BaTiO_3$ samples, scaled so that the amount of V_{Ba} in Sm-doped Ba-rich $BaTiO_3$ is equal to 1.

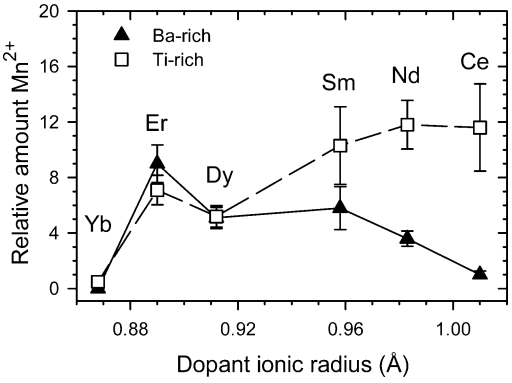

Figure 7. Relative amounts of Mn^{2+} in Ba- or Ti-rich lanthanide-doped $BaTiO_3$ samples, scaled so that the amount of Mn^{2+} in Ce-doped Ba-rich $BaTiO_3$ is equal to 1.

regardless of lanthanide dopant or concentration, and second, a plot of its intensity versus lanthanide dopant concentration did not match that reported for the $Ti^{3+}-Ln^{3+}$ complex.[33] Finally, we note the small, sharp sextet of hyperfine lines. Fitting this portion of the spectrum using powder pattern simulations revealed that $g = 2.001$ and $|A| = 0.0081 \pm 0.0001$ cm^{-1}. Consequently, we assign this signal to Mn^{2+},[17,34,35] and not Mn^{3+} or Mn^{4+}.[36,37]

In this study, the above-mentioned g values and hyperfine constants are typical of the signals for V_{Ti}, V_{Ba}, and Mn^{2+} regardless of the lanthanide dopant. In Figures 5−7 we plot the relative amounts (equivalent to the doubly integrated intensity) of V_{Ti}, V_{Ba}, and Mn^{2+} for the various samples where the signals could be measured. Though we refrain from making direct comparisons between doubly integrated signal intensities from different species, we do note that the metal vacancy signal

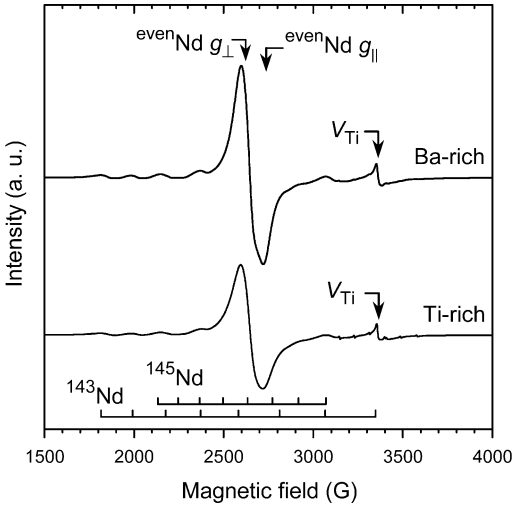

Figure 8. EPR spectra of Nd-doped $BaTiO_3$ at 10 K, where either Ba/Ti = 1.01 or 0.99.

is a very small fraction of the size of the lanthanide signal (when observed). Generally, much more V_{Ti} is measured than V_{Ba}, with the exception of Ba-rich Dy-doped and both varieties of Er-doped samples, where the amounts are in the same range. In addition, the Mn^{2+} doubly integrated intensity is generally the smallest. Uncertainties on the V_{Ba} amounts are rather large, as its signal was small (a factor of 10−100 times less) relative to the V_{Ti} and more exact determinations were not possible.

Within the uncertainty limits of our measured amounts, we see the same amounts of V_{Ti} in both Ba- and Ti-rich samples and the same amounts of V_{Ba} in both Ba- and Ti-rich samples doped with Ce. We do, however, see a marked difference in the amount of Mn^{2+}, with the Ti-rich sample having almost 12 times that of the Ba-rich sample. Though one initially would expect more Ti to cause the Mn^{2+} amount to decrease relative to the Ba-rich sample because Mn^{2+} is a B-site dopant,[34] the presence of more Ce^{3+} on the A-site requires additional compensation by acceptors such as Mn^{2+} on the B-site. We are assuming that the total amount of Mn (which likely arises from our Ti source) is roughly constant. In the case of Ce doping, driving the Ce into the A-site by B-rich conditions drives more Mn to its 2+, rather than 3+, state.

Nd^{3+}-Doping. The electronic configuration of Nd^{3+} is $4f^3$ with a free-ion ground state of $^4I_{9/2}$. The calculations above indicate that the ground state is Γ_6 regardless of A- or B-site substitution (see Table 3). Note, however, that for Nd^{3+} on the B-site, our point charge model calculates a value of x and W close to where the Γ_8 state becomes lowest.

Figure 8 shows the EPR spectra of Nd^{3+} in Ba- and Ti-rich $BaTiO_3$. Samples containing only 0.1 mol % Nd spectra were also examined, but these were essentially the same as the 1 mol % samples, excepting that the higher concentration had broader signals with some overlap. Computer powder pattern simulations revealed that the spectral parameters were essentially the same as those determined by Possenriede et al. for Nd^{3+} in $BaTiO_3$.[13] In our experiments with Ba-rich $BaTiO_3$, the even-numbered Nd isotopes yielded a signal with $g_\perp = 2.580$ and $g_\parallel = 2.464$. Hyperfine lines for ^{143}Nd and ^{145}Nd (both $I = {}^7/_2$) were identified, in a ratio of intensities approximating that of their isotopic abundance. For ^{143}Nd values of $|A_\perp| \sim 266 \times 10^{-4}$ cm^{-1} and $|A_\parallel| \sim 250 \times 10^{-4}$ cm^{-1} and for ^{145}Nd values of $|A_\perp| \sim 162 \times 10^{-4}$ cm^{-1} and $|A_\parallel| \sim 155 \times 10^{-4}$ cm^{-1} fit the powder pattern well. As the figure shows, not all the hyperfine lines were observed, as some overlapped with the signals from V_{Ti}

and even-numbered Nd^{3+} isotopes. A weighted average of the g values obtained, $^1/_3(g_{||} + 2g_\perp) = 2.541$, is close to the value of 2.667 expected for a Γ_6 state.

The spectrum when Ba/Ti = 0.99 is similar to when Ba/Ti = 1.01, with the exception that the signal from Nd^{3+} is smaller in intensity and broader. Double integration and powder pattern simulations indicated that there was about 5% more Nd^{3+} in the Ti-rich sample, a difference within our estimated error of ±10%. The same amount of Nd^{3+} in each type of sample is not unexpected given that for either type of site substitution a Γ_6 state is expected. Consequently, our EPR results on Nd^{3+} tell us little about its site substitution. Previously, ionic radii[13] and charge compensation arguments[38] have been used to suggest that Nd^{3+} is an A site dopant.

Quantification of the V_{Ti} signal was difficult here as one of the hyperfine lines from ^{143}Nd overlaps it.[39] Powder pattern simulations were used to estimate the contribution from the highest field ^{143}Nd hyperfine so that we could roughly quantify the amount of V_{Ti} present. As a consequence of the large error in this particular measurement, we cannot decisively differentiate the amount of V_{Ti} in each sample type, nor can we do so for V_{Ba}. Interestingly, we saw 3 times more Mn^{2+} in Ti-rich than in Ba-rich Nd-doped $BaTiO_3$ (see Figure 7). Like Ce-doped Ti-rich $BaTiO_3$, more Mn^{2+} in the Ti-rich sample suggests the added need for compensation by acceptors.

Sm^{3+}-Doping. The electronic configuration of Sm^{3+} is $4f^5$ with a free-ion ground state of $^6H_{5/2}$. The cubic crystal field splitting is the same as that for Ce^{3+}. Our calculations (see Table 3) predict that A site Sm^{3+} has a Γ_8 ground state, whereas B site Sm^{3+} has a ground state of Γ_6, with a g value of 1.429.

Experimentally, no signal was observed for Sm^{3+} in either Ba-rich or Ti-rich samples, though magnetic field scans were performed to field levels equivalent to g values as low as $^1/_2$. This suggests either that, at the EPR measurement temperature of 10 K, the Sm in $BaTiO_3$ is largely Sm^{2+} or that the signal from the Sm^{3+} is too broad to be detected. Though Sm^{3+} has not previously been studied in $BaTiO_3$ by EPR, it has been studied by luminescence and found to be amphoteric, occupying both A- and B-sites in $BaTiO_3$.[11] Furthermore, Sm^{3+} at the Ti^{4+} site was found to have a cubic crystal field regardless of the $BaTiO_3$ crystal symmetry (e.g., rhombohedral, orthorhombic, tetragonal, or cubic).[40]

There were approximately equivalent amounts of V_{Ti} in A- and B-rich samples and equivalent amounts of V_{Ba} in both types of sample. We did see, however, 2 times more Mn^{2+} in Ti-rich Sm-doped $BaTiO_3$. Earlier XRD results performed on the same sample batch suggest that Sm in $BaTiO_3$ is largely 3+ on the A-site at room temperature and above. More Mn^{2+} in the Ti-rich sample can therefore be rationalized by the added need for acceptors in that sample as compared to the Ba-rich sample.

Eu^{2+}-Doping. Divalent Eu is $4f^7$ with a free-ion ground state of $^8S_{7/2}$. For a pure $^8S_{7/2}$ state, the only nonzero interaction in a magnetic resonance experiment is the Zeeman splitting. S-state ions are much less sensitive to the crystal field than other ions, being only affected by second-order interactions.[20] Unlike the other Kramers (i.e., odd number of electrons) rare-earth ions, Eu^{2+} has a relatively long relaxation time, making it observable at higher temperatures, including room temperature.

The samples containing europium ions were fired under reducing conditions to ensure that as much Eu as possible was in the +2 valence state. Spectra were taken at room temperature (294 K), 253, 168, and 10 K. Figure 9 shows the Ba- and Ti-rich samples at 10 K only. The other spectra were essentially identical to those taken by Takeda.[14] Takeda identified the lattice position of Eu^{2+} as A-site, due to its similarity to A-site Gd^{3+}.

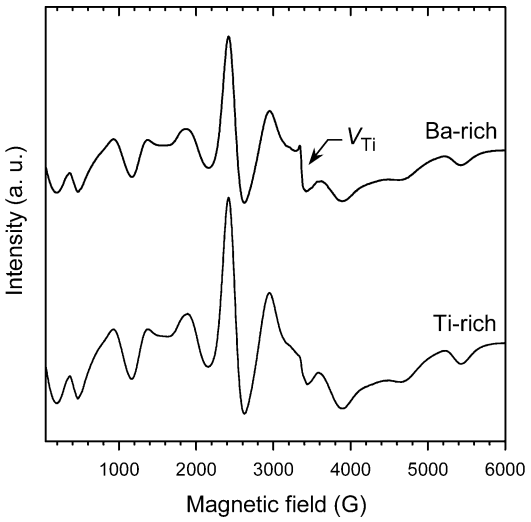

Figure 9. EPR spectra of Eu-doped, reduced $BaTiO_3$ at 10 K, where either Ba/Ti = 1.01 or 0.99. The location of a small signal due to V_{Ti} is marked at $g = 2.004$. The other features are from Eu^{2+}.

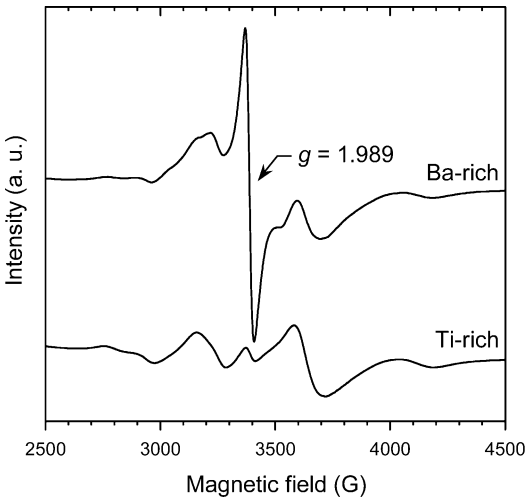

Figure 10. EPR spectra of Gd-doped $BaTiO_3$ at 10 K, where either Ba/Ti = 1.01 or 0.99. The signal at $g = 1.989$ results from Gd^{3+} primarily in the B-site, whereas the other features result from Gd^{3+} in the A-site.

The Ti-rich sample's spectra is nearly the same as those from the Ba-rich sample at each of the examined temperatures. It is slightly larger in intensity (1.3×), indicating that the excess Ba dislodges some, but not a majority of, the Eu^{2+} from its position as an A-site dopant. There is a signal from V_{Ti} at g ~ 2.004 that is visible only when Ba/Ti = 1.01. Due to the size of the Eu^{2+} signal relative to the V_{Ti}, quantification is not possible other than to note there is more V_{Ti} in the Ba-rich sample.

Gd^{3+}-Doping. Trivalent Gd^{3+} is $4f^7$ with a free-ion ground state of $^8S_{7/2}$. It is isoelectronic with Eu^{2+}. Like Eu^{2+}, the effect of the cubic crystal field should only be felt through second-order and higher effects. Also like Eu^{2+}, its relaxation is relatively slow, allowing it to be observed by EPR at higher temperatures than other rare earth ions.

EPR spectra of Ba- or Ti-rich $BaTiO_3$ were taken at 10 or 50 K (rhombohedral phase) doped with either 1 or 0.1 mol % Gd. Signals in the EPR spectra with 1 mol % Gd were slightly broadened relative those in the 0.1% spectra. Figure 10 shows spectra of both Ba- and Ti-rich material at 10 K. It can be seen that the intensity of the feature at $g = 1.989$ increases

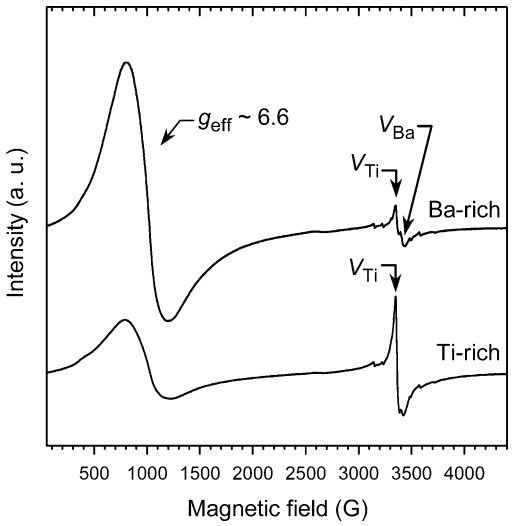

Figure 11. EPR spectra of Dy-doped $BaTiO_3$ at 10 K, where either Ba/Ti = 1.01 or 0.99. The peak at $g_{eff} \sim 6.6$ is due to Dy^{3+} at the B-site.

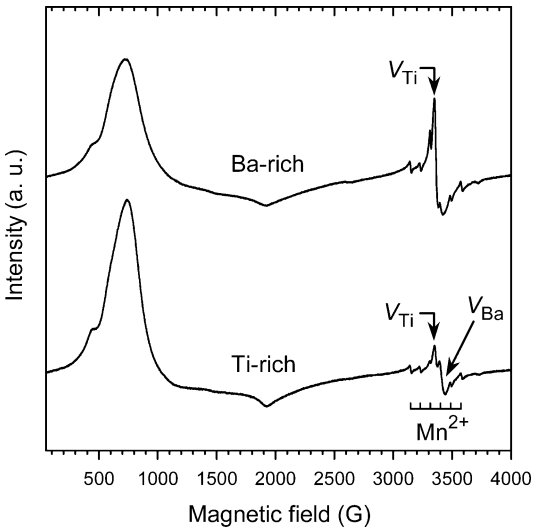

Figure 12. EPR spectra of Er-doped $BaTiO_3$ at 10 K, where either Ba/Ti = 1.01 or 0.99. The broad features between 50 and 2500 G result from Er^{3+}.

dramatically when the amount of barium in the sample is increased. Takeda and Watanabe studied Gd^{3+} in $BaTiO_3$ extensively and discerned that there are two types of Gd^{3+} spectra in $BaTiO_3$.[41] One type was assigned to Gd^{3+} in A-sites on the basis of electric field gradient calculations.[14] The other type arises from Gd^{3+} in sites with a cubic crystalline electric field in the rhombohedral, orthorhombic, tetragonal, and cubic phases of $BaTiO_3$.[14,42] This site has been assigned to Gd^{3+} substituting for Ti^{4+}, on the basis of (a) its persistent cubic symmetry, (b) doping studies, and (c) high-temperature reduction studies.[42] Consequently, interpretation of our results, though powder patterns, are not difficult. In Figure 10, broad features higher and lower than $g = 1.989$ are mainly from the different M_S transitions of Gd^{3+} in the A site, whereas the sharp line at $g = 1.989$ arises chiefly from the $M_S + {}^1/_2 \rightarrow -{}^1/_2$ transition of Gd^{3+} at the B-site.[14,41]

As Takeda and Watanabe have shown,[43] and our EPR results reconfirm, Gd^{3+} is an amphoteric ion in $BaTiO_3$. It can be forced into either A or B sites depending upon the Ba/Ti ratio, the presence of other cations occupying Ba^{2+} or Ti^{4+} sites, and finally, upon oxidative or reductive preparation conditions.[42,43] Unfortunately, because of the dominance of the Gd^{3+} spectra around $g = 2$, no information is available regarding changes in V_{Ti}, V_{Ba}, or Mn^{2+} with regard to the Ba/Ti ratio.

Dy^{3+}-Doping. We now return to our discussion of non-S-state Kramers ions, continuing with Dy^{3+}, whose electronic configuration is $4f^9$, with a free-ion ground state of ${}^6H_{15/2}$. Our point charge calculation predicts Γ_8 for Dy^{3+} in the A-site and Γ_6 for the B-site ($g_{\Gamma 6} = 6.667$) ground states (see Table 3). Dy^{3+} has not, to our knowledge, been observed in $BaTiO_3$ before by EPR.

The EPR spectra of Dy-doped Ba- and Ti-rich barium titanate are shown in Figure 11. A large, broad, anisotropic peak, with $g \sim 6.6$ due to Dy^{3+} is visible. No hyperfine lines from ^{161}Dy and ^{163}Dy are visible, most likely because of the broadness of the Dy^{3+} signal relative to the expected hyperfine coupling constants.[44] The g value of Dy^{3+} observed in Ba-rich $BaTiO_3$ corresponds to Dy^{3+} in the B site. However, no signal from the A-site Dy^{3+} is apparent.

The intensity of the Dy^{3+} is strongly dependent upon the Ba/Ti ratio, with the Ba-rich sample showing 3 times the Dy^{3+} signal as compared to the Ti-rich (Figure 11). The decrease in Dy^{3+} intensity as the Ti concentration increases matches what one would expect for a B site dopant. A-site Dy^{3+} could be reduced to Dy^{2+} at low temperature by capture of an electron, thus making it invisible to EPR. The higher V_{Ti} signal in the Ti-rich sample demonstrates the need for acceptors and suggests that during the incorporation, at high temperature, the Dy valence is 3+ on the A-site also.

The V_{Ti} and V_{Ba} signals have an interesting dependence upon whether the sample is Ba- or Ti-rich. Ti-rich $BaTiO_3$ has 4 times the V_{Ti} signal but only two-fifths the V_{Ba} as compared to Ba-rich (Figures 11 and 6). Dy^{3+} on a B-site (Dy_{Ti}') acts as an acceptor. In Ba-rich samples, there is more Dy_{Ti}', so there is less need for compensation by V_{Ti}. Consequently, we see less V_{Ti} when Ba/Ti = 1.01. Though V_{Ba} is also a metal vacancy and there is less need for them in terms of compensation in the Ba-rich sample, we see more. This must now be a result of Dy's preference for the B-site, specifically, when Ba/Ti = 1.01, then Ba/(Ti + Dy_{Ti}') < 1, requiring the lattice to adjust for an overabundance of atoms on the B-site.

Er^{3+}-Doping. The electronic configuration of Er^{3+} is $4f^{11}$, with a free-ion ground state of ${}^4I_{15/2}$. Our point charge model calculation predicts a Γ_8 level ground state (albeit different ones) for both A and B site substitution (see Table 3).[45] To our knowledge, Er^{3+} has not been observed in $BaTiO_3$ by EPR previously.

Figure 12 shows the experimental spectrum of Er in both Ba- and Ti-rich $BaTiO_3$. The Er^{3+} signal arises from either an Er^{3+} environment with axial symmetry or a cubic symmetry environment with a Γ_8 ground state. Because we are limited in this study to examining $BaTiO_3$ powders, we cannot discern with certainty whether this signal arises from Er^{3+} either in a Γ_8 level of a cubic environment or in a lower symmetry environment. Computer powder pattern fitting of $g_{||}$, $g_{\perp}$, their widths, and line shapes, suggests that $g_{||} \sim 8.6$ and $g_{\perp} \sim 3.9$. In this fit, the breadth of $g_{\perp}$ is 1000 G, 4 times that of $g_{||}$. The width and position of $g_{\perp}$ allows for a broad, low intensity negative signal in the spectrum, fitting the experimental result acceptably. Such a fit runs counter to intuition, as judging from the height of the signals, one would be tempted to assign $g_{\perp}$ to the feature at $g \sim 8.6$. However, in simulations employing $g_{\perp} = 8.6$, we could not find values for $g_{||}$ and the two line widths that yielded a fit to the experimental spectrum.

In comparing Ba-rich to Ti-rich samples, we see about 0.7 Er^{3+} in Ba-rich $BaTiO_3$ for every one Er^{3+} in Ti-rich material.

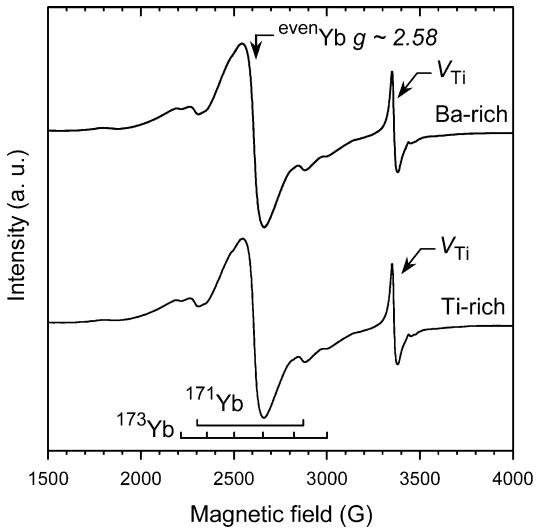

Figure 13. EPR spectra of Yb-doped $BaTiO_3$ at 10 K, where either Ba/Ti = 1.01 or 0.99.

Because Er is not likely to form a 2+ ion by capture of an electron at low temperature, such an observation suggests that the Er^{3+} signal we observe arises from Er^{3+} on the A-site. Further analysis of Er-doped $BaTiO_3$ single crystals is necessary to confirm the origin of these interesting signals.

On the basis of previous XRD work[6,7,46] and other studies,[4,47] Er^{3+} is amphoteric with a preference for the B-site. Thus, we can interpret the amounts of V_{Ti}, V_{Ba}, and Mn^{2+} in the two types of samples. Er^{3+} on the B-site is an acceptor, whereas A-site Er^{3+} is a donor. When Ba/Ti = 1.01, we anticipate having more B-site Er^{3+} (more acceptors). In accord with this, we see less than one-third the titanium vacancies (which are also acceptors) when Ba/Ti = 1.01 than when Ba/Ti = 0.99. We see essentially the same amounts of V_{Ba} and the same amounts of Mn^{2+} for each type sample.[48]

Yb^{3+}-Doping. The Yb^{3+} ion is $4f^{13}$ with a free-ion ground state of $^2F_{7/2}$. The point charge model calculations predict that it will be in a Γ_8 quartet for A-site substitution whereas B-site substitution will lead to a Γ_6 doublet, with a predicted g value of 2.67 (see Table 3). Previously, Yb^{3+} has been observed in octahedral coordination in alkaline earth oxides with a g value of 2.57−2.59;[44] in $SrTiO_3$ as a Γ_6 doublet with $g_{\parallel} \sim 2.2$ and $g_{\perp} \sim 2.7$;[25] and, interestingly, in $KTaO_3$, as an A-site cation when codoped with uranium.[15] Apparently, EPR signals from Yb^{3+} in $BaTiO_3$ have not previously been reported.

For Ba-rich Yb-doped $BaTiO_3$ samples, we see prominent signals from Yb^{3+} and V_{Ti}. (See Figure 13.) The Yb^{3+} signal is approximately isotropic, appearing at a g value of 2.58, with hyperfine lines from ^{171}Yb ($I = {}^1/_2$) and ^{173}Yb ($I = {}^5/_2$) appearing. The lower experimental g value than the theoretical can be ascribed to covalent interactions, as in the case of Yb^{3+} in CaO.[49] Through computer-based powder pattern simulations, it was determined that the hyperfine coupling constants of the ^{171}Yb and ^{173}Yb were approximately those typical of Yb in an octahedron of oxygen atoms, where $A(^{171}Yb) \sim 6.9 \times 10^{-2}$ cm^{-1} and $A(^{173}Yb) \sim 1.9 \times 10^{-2}$ cm^{-1}.[44] The ratio of intensities fit the natural abundance of Yb isotopes well. Because of its g value indicating a Γ_6 ground state, we assign the Yb^{3+} to the B-site in $BaTiO_3$.

The Ti-rich sample yielded a very similar EPR spectrum to the Ba-rich sample. The intensities of the Yb^{3+} in each sample type are equal, as are the intensities of the V_{Ti} signals. This is somewhat puzzling, as we would expect the Ti-rich sample to have somewhat reduced Yb^{3+} intensity, but it may be that even an excess of Ti is not sufficient to remove Yb from the B-site. The large size of the V_{Ti} signal is also puzzling, as Yb_{Ti}' is an acceptor. A very small amount of Mn^{2+} was observed in the Ti-rich sample, whereas none was observed in Ba-rich samples.

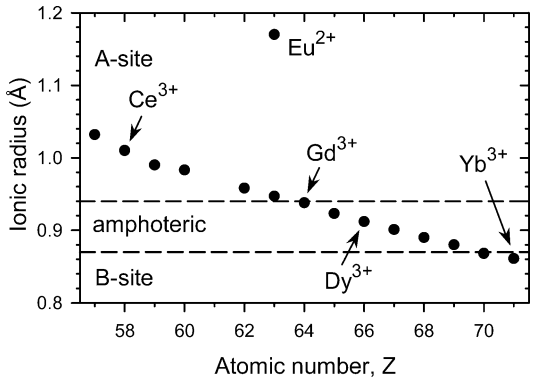

Figure 14. Plot of atomic number versus ionic radii for lanthanide 3+ ions for 6-fold coordination. The dashed lines divide the plot into regions of A-site occupancy, amphoteric behavior, and B-site occupancy, as determined from refs 6 and 7. The dopants whose site occupancy has been identified by EPR are labeled. The site occupancy as determined by EPR agrees with our earlier conclusions determined by XRD.

Discussion

The results of this paper and other known lanthanide site assignments in $BaTiO_3$ are summarized in Figure 14. In that figure, we also compare these results to a recent X-ray diffraction (XRD) volume difference study on lanthanide dopants in $BaTiO_3$.[6,7] We plot the dopant ionic radius[50] in 6-fold coordination versus dopant atomic number, dividing the plot into three regimes of occupancy, on the basis of the above-mentioned XRD results. In summary, the XRD study found that dopants with ionic radii lower than 0.87 Å are B-site, dopants with ionic radii greater than 0.94 Å are A-sites and those between are amphoteric. We note that the powders were fired in reducing atmosphere in the XRD work but are air-fired in this EPR study. Site occupancy will be influenced by oxygen partial pressure via oxygen vacancies in the lattice.[6,7] As a consequence, the "band of amphotericity" should be pushed toward larger ionic radii for air-fired samples. Technologically, this may be important when developing compositions for capacitors when considering amphoteric dopants[2] for dielectrics in capacitor constructions using nickel, copper, or other base metal electrodes.

Furthermore, for the two cations studied here with the largest diameter, specifically Eu^{2+} and Ce^{3+}, we find that the dopant ion signal depends on the Ba/Ti ratio. This, however, is not evidence for amphotericity. It appears that the Ba-rich samples have a lower amount of either ion due to oxidation to a higher charge state, which is then invisible to EPR. Gd^{3+}, studied by EPR by Takeda,[14] has been shown to be amphoteric and reconfirmed by this investigation. The quantitation of signals from Gd_{Ti}' versus $Gd_{Ba}^{\bullet}$ is difficult, but it appears that there is only a small fraction of the observed Gd^{3+} as Gd_{Ti}' (on the Ti-site) in the Ba-rich sample. The XRD study of reduced powders[6,7] also demonstrated amphoteric behavior for Gd^{3+} in $BaTiO_3$ and its preference for the A-site. Dy^{3+} in this study shows behavior explainable by amphotericity, though more clear proof would be obtained if both the Γ_6 (B-site) and Γ_8 (A-site) states were visible. Finally, for Yb^{3+}, we only see by EPR evidence for the B-site, again regardless of Ba/Ti ratio.

It should be noted that several difficulties prevented us from assigning the boundaries between A- or B-site behavior and amphotericity as precisely as the XRD data. Foremost is the fact that EPR is largely constrained to examine Kramers ions (odd number of electrons). Second, difficulties with the site assignment of Nd^{3+} and the inability to see Sm^{3+} by EPR prevented us from addressing the A-site to amphotericity boundary at all. For Nd^{3+}, we could not discern A-site versus B-site by simple EPR arguments, as the same fundamental level is predicted for both dopant sites, and, Ba- and Ti-rich samples have approximately the same amount of Nd^{3+}. Despite previous studies suggesting an A-site occupancy,[38] we were not able to identify amphotericity or lack thereof from the present EPR study. Though no Sm^{3+} EPR signal was detected, Sm^{3+} has been found to be amphoteric in air-fired, very pure $BaTiO_3$,[11] consequently supporting the notion that air-firing shifts the "band of amphotericity" to larger ionic radii. Finally, by powder pattern EPR we are unable to identify the exact nature of the signal arising from Er^{3+}, and thus the amphoteric to B-site transition is not well-defined either. As a result, although our EPR results generally agree with the XRD data, they do not give us enough data to discern any difference from air versus reductive atmosphere firing in the location of the "band of amphotericity".

With the exception of the Yb-doped samples, the samples examined in this study have defect chemistries that reflect the site the dopant prefers. In Figure 5, samples that are doped with lanthanides that prefer the A-site (Ce, Nd, and Sm) all have titanium vacancy EPR signals and have intensity levels generally higher than the two more amphoteric dopants (Dy and Er) regardless of the Ba/Ti ratio. Furthermore, Er-doped and Ba-rich Dy-doped samples have higher levels of V_{Ba} relative to samples which strictly prefer the A-site (Ce, Nd and Sm), indicating the filling of barium lattice positions by the large radii lanthanides (Ce, Nd, and Sm).

The EPR signal from Mn^{2+} appears to depend on both the dopant site preference and the Ba/Ti ratio, as shown in Figure 7. Although we have not intentionally doped these samples with manganese, it is likely a relatively constant impurity in the TiO_2 (or $BaCO_3$) precursors. Although it is known that the valence state of Mn in air-fired $BaTiO_3$ doped solely with Mn is predominantly 3+ and 4+,[51] the presence of donors can enable Mn^{3+} to capture an electron, resulting in Mn^{2+}.[34] Furthermore, samples doped with 0.1% Nd showed approximately 6−20% of the Mn^{2+} as samples doped with 1% Nd. Clearly, the amount of Mn^{2+} visible is linked to the degree of donor behavior. As Figure 7 shows, those samples where lanthanides are preferentially in the A-site (e.g., Ti-rich $BaTiO_3$ doped with Ce, Sm, or Nd) have the highest amount of Mn^{2+}. When a lanthanide that functions only as an acceptor (Yb^{3+}) is the dopant, very little Mn^{2+} is observed. It is possible that neither Mn^{3+} nor Mn^{4+} are observed in any of the samples studied here, particularly those doped with Yb, due to either the overlap from the much stronger lanthanide signal or the Mn in the higher oxidation state having significantly broader line width.[35] Because Mn is an unintentional dopant, and likely quite low in concentration, further interpretation of Figure 7 is not warranted.

Conclusions

Through theoretical predictions and experimental EPR measurements, we investigated the site substitution of certain lanthanide dopants in $BaTiO_3$. We identified Yb^{3+} as being a B-site dopant regardless of Ba/Ti ratio. We also identified Dy^{3+} as being B-site, with a signal intensity behavior that suggests amphotericity consistent with X-ray diffraction studies. In accord with previous EPR literature results, we confirmed the amphoteric behavior of Gd^{3+} and the A-site substitution of Eu^{2+}. The intensity of the Ce^{3+} signal depended upon the Ba/Ti ratio such that it implies it is mainly an A-site dopant. When driven to the B-site, as in A-rich chemistries, Ce is likely 4+, consequently invisible to EPR. Though EPR spectra were recorded for Nd^{3+} and Er^{3+}, it was not clear which sites they take solely from their EPR spectra. In Sm-doped samples, no signal attributable to either site was recorded. The site assignments that could be made via EPR matched well with our previous XRD studies. In general, the levels of metal vacancies also tracked with the site preference of the dopant. Samples with A-site dopants (Ce, Nd, and Sm) had more titanium vacancies and fewer barium vacancies than samples with amphoteric dopants (Er and Dy).

Acknowledgment. Sandia National Laboratories is a multiprogram laboratory operated by Sandia Corporation, a Lockheed Martin Co. This work was supported by the United States Department of Energy under Contract DE-AC04-94AL85000 with partial support from the National Science Foundation I/UCRC program. We wish to thank Dr. Paul Clem for initiating the collaboration between the EPR lab at Sandia and Penn State and for fruitful discussions with him.

References and Notes

(1) Lee, W. H.; Groen, W. A.; Schreinemacher, H.; Hennings, D. *J. Electroceram.* **2000**, *5*, 31.
(2) Tsur, Y.; Randall, C. A. *AIP Conf. Proc.* **2000**, *535*, 283.
(3) Hennings, D. F. K. *J. Eur. Ceram. Soc.* **2001**, *21*, 1637 and references therein.
(4) Takada, K.; Chang, E.; Smyth, D. M. *Adv. Ceram.* **1986**, *19*, 147.
(5) Xue, L. A.; Chen, Y.; Brook, R. J. *Mater. Sci. Eng.* **1988**, *B1*, 193.
(6) Tsur, Y.; Hitomi, A.; Scrymgeour, I.; Randall, C. A. *Jpn. J. Appl. Phys., Part 1* **2001**, *40*, 255.
(7) Tsur, Y.; Dunbar, T. D.; Randall, C. A. *J. Electroceram.* **2001**, *7*, 25.
(8) Buscaglia, M. T.; Buscaglia, V.; Viviani, M.; Nanni, P.; Hanuskova, M. *J. Eur. Ceram. Soc.* **2000**, *20*, 1997.
(9) Lewis, G. V.; Catlow, C. R. A. *J. Phys. Chem. Solids* **1986**, *47*, 89.
(10) Buscaglia, M. T.; Buscaglia, V.; Viviani, M.; Nanni, P. *J. Am. Ceram. Soc.* **2001**, *84*, 376.
(11) Makishima, S.; Hasegawa, K.; Shionoya, S. *J. Phys. Chem. Solids* **1962**, *23*, 749.
(12) Schwartz, R. N.; Wechsler, B. A. *Phys. Rev. B* **2000**, *61*, 8141.
(13) Possenriede, E.; Schirmer, O. F.; Godefroy, G. *Phys. Status Solidi B* **1990**, *161*, K55.
(14) Takeda, T. *J. Phys. Soc. Jpn.* **1968**, *24*, 533.
(15) Abraham, M. M.; Boatner, L. A.; Olson, D. N.; Höchli, U. T. *J. Chem. Phys.* **1984**, *81*, 2528.
(16) Yamaka, E. *J. Phys. Soc. Jpn.* **1963**, *18*, 1557.
(17) Ikushima, H. *J. Phys. Soc. Jpn.* **1966**, *21*, 1866.
(18) Tsur, Y.; Randall, C. A. *Proc. Electrochem. Soc.* **2000**, *99−38*, 502.
(19) Tsur, Y.; Randall, C. A. *J. Am. Ceram. Soc.* **2001**, *84*, 2147.
(20) Abragam, A.; Bleaney, B. *Electron Paramagnetic Resonance of Transition Ions*; Clarendon Press: Oxford, U.K., 1970.
(21) Lea, K. R.; Leask, M. J. M.; Wolf, W. P. *J. Phys. Chem. Solids* **1962**, *23*, 1381.
(22) Bureau, B.; Silly, G.; Buzare, J. Y. *J. Phys. Chem. Solids* **1998**, *59*, 951.
(23) Siegel, E.; Müller, K. A. *Phys. Rev. B* **1979**, *20*, 3587.
(24) For the rhombohedral phase, $a = 4.004$ Å and $\alpha = 89.97°$ at 132 K. (See ref 23.) Such a unit cell requires only a very small distortion from cubic, compressing three cube diagonals by 0.08% and lengthening one by 0.2%.
(25) Rimai, L.; DeMars, G. A. Electron paramagnetic resonance of some rare earth impurities in strontium titanate. In *Paramagnetic Resonance, Proceedings of the first international conference held in Jerusalem, July 16−20, 1962*; Low, W., Ed.; Academic Press: New York, 1963; pp 51−58.
(26) Devine, R. A. B.; Berthier, Y. *Solid State Commun.* **1978**, *26*, 315.
(27) Newman, D. J. *Adv. Phys.* **1971**, *20*, 197.
(28) Reynolds, R. W.; Chen, Y.; Boatner, L. A.; Abraham, M. M. *Phys. Rev. Lett.* **1972**, *29*, 18.

(29) Makovec, D.; Samardzija, Z.; Kolar, D. *J. Solid State Chem.* **1996**, *123*, 30.

(30) Possenriede, E.; Jacobs, P.; Schirmer, O. F. *J. Phys.: Condens. Matter* **1992**, *4*, 4719 and references therein.

(31) Glinchuk, M. D.; Bykov, I. P.; Kornienko, S. M.; Laguta, V. V.; Slipenyuk, A. M.; Bilous, A. G.; V'yunov, O. I.; Yanchevskii, O. Z. *J. Mater. Chem.* **2000**, *10*, 941.

(32) Kolodiazhnyi, T.; Petric, A. *J. Phys. Chem. Solids* **2003**, *64*, 953.

(33) Kornienko, S. M.; Bykov, I. P.; Glinchuk, M. D.; Laguta, V. V.; Belous, A. G.; Yastrabik, L. *Phys. Solid State* **1999**, *41*, 1688.

(34) Nakahara, M.; Murakami, T. *J. Appl. Phys.* **1974**, *45*, 3795.

(35) Milsch, B. *Phys. Status Solidi A* **1992**, *133*, 455.

(36) Müller, K. A.; Berlinger, W.; Blazey, K. W.; Albers, J. *Solid State Commun.* **1987**, *61*, 21.

(37) Serway, R. A.; Berlinger, W.; Müller, K. A.; Collins, R. W. *Phys. Rev. B* **1977**, *16*, 4761.

(38) Abdulsabirov, R. Y.; Falin, M. L.; Fazlizhanov, I. I.; Kazakov, B. N.; Korableva, S. L.; Ibragimov, I. R.; Safiullin, G. M.; Yakovleva, Zh. *Appl. Magn. Reson.* **1993**, *5*, 377.

(39) Note added in review: Raising the temperature of the sample would broaden the Nd^{3+} EPR signal to the point where it would no longer obscure the V_{Ti} and V_{Ba} signals, thus allowing for more precise measurement of each signal in each type of Nd-doped sample.

(40) Makishima, S.; Yamamoto, H.; Tomotsu, T.; Shionoya, S. *J. Phys. Soc. Jpn.* **1965**, *20*, 2147.

(41) Takeda, T.; Watanabe, A. *J. Phys. Soc. Jpn.* **1964**, *19*, 1742.

(42) Takeda, T.; Watanabe, A. *J. Phys. Soc. Jpn.* **1966**, *21*, 1132.

(43) Takeda, T.; Watanabe, A. *Jpn. J. Appl. Phys.* **1968**, *7*, 232.

(44) Reynolds, R. W.; Boatner, L. A.; Chen, Y.; Abraham, M. M. *J. Chem. Phys.* **1974**, *60*, 1593.

(45) The two predicted Γ_8 levels are not the same, however, and could perhaps be differentiated through careful EPR investigations of single-crystal samples.

(46) Buscaglia, M. T.; Viviani, M.; Buscaglia, V.; Bottino, C.; Nanni, P. *J. Am. Ceram. Soc.* **2002**, *85*, 1569.

(47) Rotenberg, B. A.; Danilyuk, Y. L.; Gindin, E. I.; Prokhvatilov, V. G. *Sov. Phys.-Solid State* **1966**, *7*, 2465.

(48) In Er-doped, Ba-rich $BaTiO_3$ the line shape of the large V_{Ti} signal makes the peak to peak height difference of the V_{Ba} signal in the Ba-rich material look small in comparison to that of the Ti-rich material. Simulations reveal that there is about the same amount of V_{Ba} signal in each.

(49) Low, W.; Rubins, R. S. *Phys. Rev.* **1963**, *131*, 2527.

(50) Shannon, R. D. *Acta Crystallogr. A* **1976**, *32*, 751.

(51) Hagemann, H. J.; Ihrig, H. *Phys. Rev. B* **1979**, *20*, 3871.